Desalination and Water Treatment
www.deswater.com
doi: 10.5004/dwt.2019.23814

154 (2019) 195–200
June

A facile and green method of preparation of mesoporous $ZnFe_2O_4$ with enhanced adsorption activity

Mahboubeh Rabbani*, Rahmatollah Rahimi, Mahdieh Rabiei Ghadi, Mahdi Heidari-Golafzani

Department of Chemistry, Iran University of Science and Technology, Tehran 16846-13114, Iran, Tel. +98-21-77240651; Fax: +98-21-77491204; email: m_rabani@iust.ac.ir (M. Rabbani), Tel. +98-21-77240290; Fax: +98-21-77491204; emails: rahimi_rah@iust.ac.ir (R. Rahimi), mahdie.rabiei69@gmail.com (M.R. Ghadi), Tel. +98-9113478060; Fax: +98-21-77491204; email: heidarimahdi300@gmail.com (M. Heidari-Golafzani)

Received 9 March 2018; Accepted 14 January 2019

ABSTRACT

In this study, mesoporous $ZnFe_2O_4$ was prepared by a facile and green hydrothermal method. Carboxymethylcellulose is a nontoxic and water-soluble polymer that was used as surfactant. The obtained adsorbent was characterized by different techniques such as scanning electron microscopy, X-ray diffraction, vibrating sample magnetometer, Fourier-transform infrared spectroscopy and Brunauer–Emmett–Teller theory. The results indicated that $ZnFe_2O_4$ with high purity phase possesses obvious mesoporous structure; the mean inner diameter, specific surface area and pore volume are about 8.1 nm, 104.16 m^2/g and 0.21 cm^3/g, respectively. Furthermore, as-synthesized adsorbent has appropriate reusability property. So, it can be used for four runs. The adsorption properties of methylene blue (MB) onto mesoporous $ZnFe_2O_4$ were studied and the results indicated that the maximum adsorption capacity of mesoporous $ZnFe_2O_4$ for MB was 250 mg/g in a time period of only 15 min. For concentration of 10–200 ppm, removal efficiency is over 90% while this amount for 500 ppm concentration is about 63%.

Keywords: Magnetic materials; Mesoporous ferrite; CMC; Methylene blue; Adsorption; Spectroscopy

1. Introduction

Among the family of ferrites (M-Fe_2O_4), Zn ferrites have been attractive due to its numerous properties including high chemical stability, corrosion resistivity, magneto crystalline anisotropy and magneto optical attributes [1–4]. $ZnFe_2O_4$ is an *n*-type semiconductor which is recognized as an useful spinel ferrite because of its features such as environmental friendliness, photochemical stability, multiple valence and diverse properties that depend on particle size and preparation conditions [5,6]. Whereas the various applications of it are dependent on its structure, morphology and particle size, numerous studies have been done to synthesize $ZnFe_2O_4$ with different morphologies via different synthesizing methods [5]. Furthermore, porous compounds can provide effective sites for adsorption processes, therefore can be used for removal and separation of toxic organic dyes [7–10] and metal ions [11–15] from water. Among the different methods for elimination of pollutants from wastewater, adsorption process is a preferred way to remove contaminants because of its environmental friendliness and cost effectiveness. In addition, combining the above method and magnetic separation has been considered as an effective idea. Mesoporous $ZnFe_2O_4$ has an enhanced morphology with large pore volume and high surface area that was fabricated in many researches recently [1,2,5,6,16–22].

In this paper, for the first time, we have used the carboxymethylcellulose (CMC) as surfactant in order to synthesize mesoporous $ZnFe_2O_4$. CMC was used in controlling

* Corresponding author.

the size and morphology of mesoporous $ZnFe_2O_4$. Then, its adsorption of methylene blue in aqueous solution was investigated.

2. Experimental setup

2.1. Materials and methods

Mesoporous $ZnFe_2O_4$ was prepared in the presence of CMC via hydrothermal method. All the reagents used in this study were obtained from commercial sources and applied as received from Sigma-Aldrich Chemical Co., (Tehran province). Iron(III) ($Fe(NO_3)_3{\cdot}9H_2O$), zinc(II) ($Zn(NO_3)_2{\cdot}6H_2O$) and CMC were used to prepare the sample. 0.4 g of CMC was dissolved in 14 mL of $Zn(NO_3)_2{\cdot}6H_2O$ solution (0.2 M) to form a homogeneous solution. As-prepared solution was mixed with 14 mL of $Fe(NO_3)_3{\cdot}9H_2O$ solution (0.4 M) (with molar ratio of 1:2 between [Zn] and [Fe]), and then, was stirred magnetically at 0°C for 0.5 h. Sodium hydroxide solution (7.0 M) was added dropwise into the mixture until the pH reached 10.0. This solution was sonicated for 30 min and then transferred into a 100 mL round-bottom flask and kept at 130°C for 24 h in an oven. The obtained precipitate was centrifuged and washed with deionized water several times. Finally, as-prepared precipitate was dried in a vacuum oven at 75°C for 6 h.

2.2. Characterization

The morphology of $ZnFe_2O_4$ was analyzed through a scanning electron microscopy (SEM) (Seron Technology-AIS2100, Tehran). Fourier transform infrared spectroscopy (FT-IR) measurements were carried out in the wavenumber range of 400–4,000 cm^{-1} on a Shimadzu FTIR-8400S spectrophotometer (Tehran). In order to analyze the structure, powder X-ray diffractometer (XRD, Bruker AXS D8 advance, Tehran) was used. Magnetic properties of adsorbent were measured by vibrating sample magnetometer (VSM/AGFM). Nitrogen adsorption–desorption isotherms were examined using a Micromeritics ASAP 2020 M system (Tehran).

2.3. Study of adsorption properties of mesoporous $ZnFe_2O_4$

In order to investigate the adsorption capacity of the prepared mesoporous $ZnFe_2O_4$, a series of methylene blue solutions with different concentrations (10–500 mg/L) were prepared by dissolving a known amount of methylene blue into 50 mL of distilled water in different transparent containers. 0.05 g of mesoporous $ZnFe_2O_4$ was placed into 50 mL methylene blue (MB) solution under stirring (500 rpm). For determination of MB decolorization at specified periods, 3 mL of each sample was collected and separated from the adsorbent by centrifugation. The adsorbent performance was indirectly monitored by relating the optical absorbance. The absorption peaks corresponding to MB decreased gradually as the exposure time was extended.

3. Results and discussion

3.1. Characterization of mesoporous $ZnFe_2O_4$

The SEM image of mesoporous $ZnFe_2O_4$ is shown in Fig. 1a. It is obvious that $ZnFe_2O_4$ is uneven nanoparticles with a diameter of 35–65 nm and particle distribution is uniform.

It can be seen that the XRD pattern of the prepared mesoporous $ZnFe_2O_4$ is indicated in Fig. 1b, the sharp peaks at $2\theta = 29.9°$, 35.3°, 42.9°, 53.2°, 56.7° and 62.2° can be assigned to the diffraction of $ZnFe_2O_4$ crystal with (2 2 0), (3 1 1), (4 0 0), (4 2 0), (5 1 1) and (4 4 0) lattice planes, respectively (JCPDS card No. 77-0011) [2,6,7]. All diffraction peaks position match well with those of cubic spinel structure (space group $FD\bar{3}m$) of $ZnFe_2O_4$ peaks [8]. No obvious impurity phase was detected. Moreover, all marked peaks are related to $ZnFe_2O_4$. The mechanism for the formation of the zinc ferrite powders is given below [23]:

$$Zn + 2H_2O \rightarrow Zn(OH)_2 + H_2 \quad (1)$$

$$Zn(OH)_2 \rightarrow ZnO + H_2O \quad (2)$$

$$Zn + 4NH_3 + 2H_2O \rightarrow [Zn(NH_3)_4](OH)_2 + H_2 \quad (3)$$

$$ZnO + H_2O \leftrightarrow HZnO_2^- + H^+ \quad (4)$$

$$ZnO + H_2O \leftrightarrow ZnO_2^{2-} + H^+ \quad (5)$$

$$Zn(OH)_2 + nNH_3 \leftrightarrow Zn(NH_3)_n^{2+} + 2OH^- \ (n = 1-4) \quad (6)$$

$$Fe^{2+} + 2OH^- \rightarrow Fe(OH)_2 \quad (7)$$

$$Fe(OH)_2 + OH^- + O_2 + H_2O \rightarrow [Fe(OH)_n]^{-(n-3)} \ (n = 2,3) \quad (8)$$

$$\text{Soluble Zn species} + [Fe(OH)_n]^{-(n-3)} \rightarrow ZnFe_2O_4 \quad (9)$$

The general reaction could be expressed as follows:

$$Zn + FeCl_2 + NH_3.H_2O \rightarrow ZnFe_2O_4 \quad (10)$$

Fig. 1c shows the hysteresis loops of synthesized mesoporous $ZnFe_2O_4$ recorded at room temperature. It clearly indicated that when the particle size was decreased to below a critical value (lower than 100 nm), superparamagnetic behavior of the prepared samples was affected. The magnetic saturation (Ms) value of $ZnFe_2O_4$ was 2.5 emu/g [11].

In Fig. 1d, the FT-IR spectra of mesoporous $ZnFe_2O_4$ was shown in the range 400–4,000 cm^{-1}. In the $ZnFe_2O_4$ spectra, the strong and sharp absorption band emerged at 582 cm^{-1} is assigned to the stretching vibrations of M–O characteristic cubic spinel structure. Broad band in the range 3,300–3,500 cm^{-1} associated to the hydroxyl stretching. Also, the peaks at 1,417 and 1,627 cm^{-1} attributed to the symmetric and asymmetric stretching of COO^-, respectively, confirm that some of acetate ions are grafted on the surface of catalyst [3,5,7].

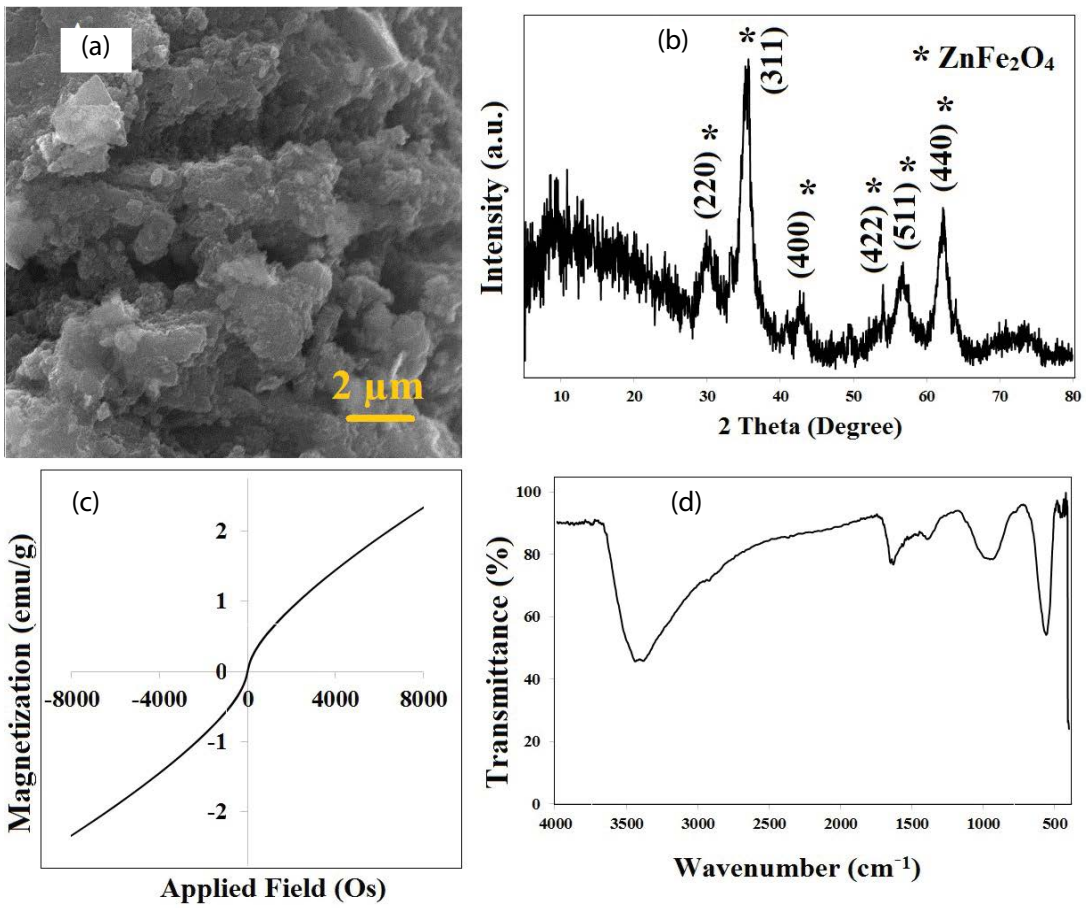

Fig. 1. (a) SEM image, (b) XRD pattern, (c) VSM curve and (d) FT-IR spectra of mesoporous $ZnFe_2O_4$.

In Fig. 2a, the nitrogen adsorption–desorption isotherm displays type IV isotherm. Distinct hysteresis loop clearly illustrated the presence of mesoporous $ZnFe_2O_4$ [2,3,5,8,9]. Furthermore, the average pore diameter of mesoporous $ZnFe_2O_4$ was determined to be 8.1 nm by Barrett-Joyner-Halenda analyses from the sorption isotherms (Fig. 2b). Specific surface area of mesoporous $ZnFe_2O_4$ around 104.16 cm^2/g and pore volume of about 0.21 cm^3/g are calculated by using Brunauer–Emmett–Teller method.

3.2. Investigation of adsorption properties of mesoporous $ZnFe_2O_4$

The adsorption properties of MB onto mesoporous $ZnFe_2O_4$ were evaluated. Fig. 3a shows the UV–Vis spectra of various concentrations of MB solutions by prepared sample. It was indicated that the MB adsorption peaks at 664 nm decreased fast and almost completely disappeared within 15 min. The removal efficiency of MB with different concentrations was shown in the inset of this figure. On the other hand, there are many holes on the adsorbent surface that causes high and stable adsorption capacity during experimental runs. Moreover, Fig. 3b shows the experimental data of Q_e vs. equilibrium concentration C_e. The results illustrated that the maximum adsorption capacity of mesoporous $ZnFe_2O_4$ for MB was 250 mg/g in a time period of only 15 min.

It is clear that the surface hydroxyl groups of the adsorbent have the main effect on the adsorption of methylene blue onto the mesoporous $ZnFe_2O_4$.

The result is presented in Fig. 3c, from which we can see that the adsorbent activity of the mesoporous $ZnFe_2O_4$ decreased awhile after each cycle. After being used for four times, the magnetic adsorbent still shows an adsorbent percentage of 96% at the same condition.

For investigation of reusability of adsorbent, after each cycle, the adsorbent has been separated magnetically, afterward dispersed in ethanol and sonicated for 15 min and washed several times with water and dried at 60°C for 8 h. The results indicated that no significant change was observed in adsorption activity. In addition, because of magnetic property, the adsorbent is easily recovered from wastewater. Fig. 3d demonstrates that the mesoporous $ZnFe_2O_4$ can be easily collected by external magnetic field.

In order to compare the adsorption rate of dyes, different amounts of catalyst were used. MB was chosen as an experimental dye. Adsorption behavior of MB at three different times in the presence of different amounts of catalyst is indicated in Fig. 4a. C_t and C_0 are concentration of dyes after different visible light irradiation times and concentration of dyes after the adsorption–desorption equilibrium is reached but before irradiation, respectively. It has been observed that the adsorption process was carried out better in lower concentrations.

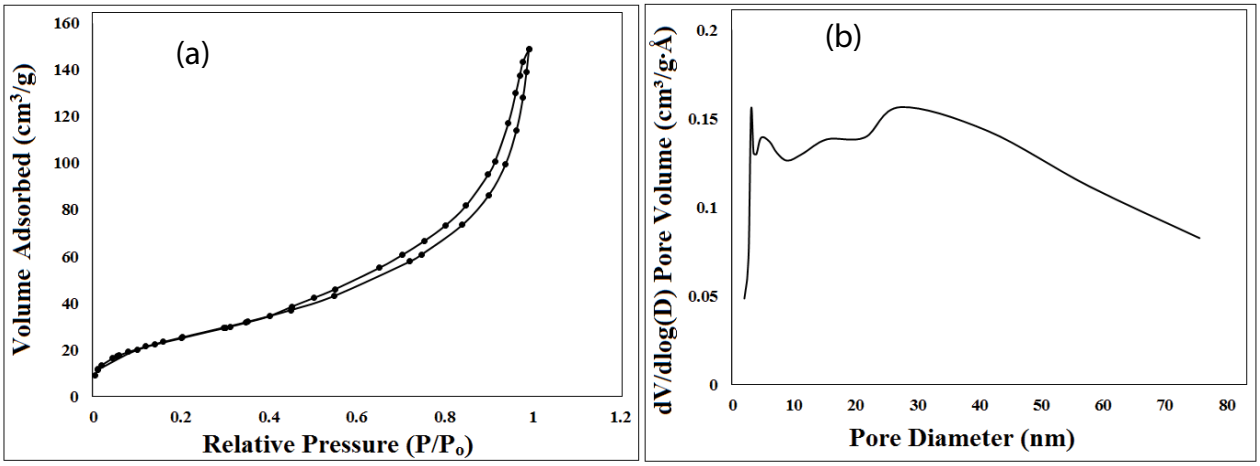

Fig. 2. (a) Nitrogen sorption isotherm and (b) pore size distribution of mesoporous $ZnFe_2O_4$.

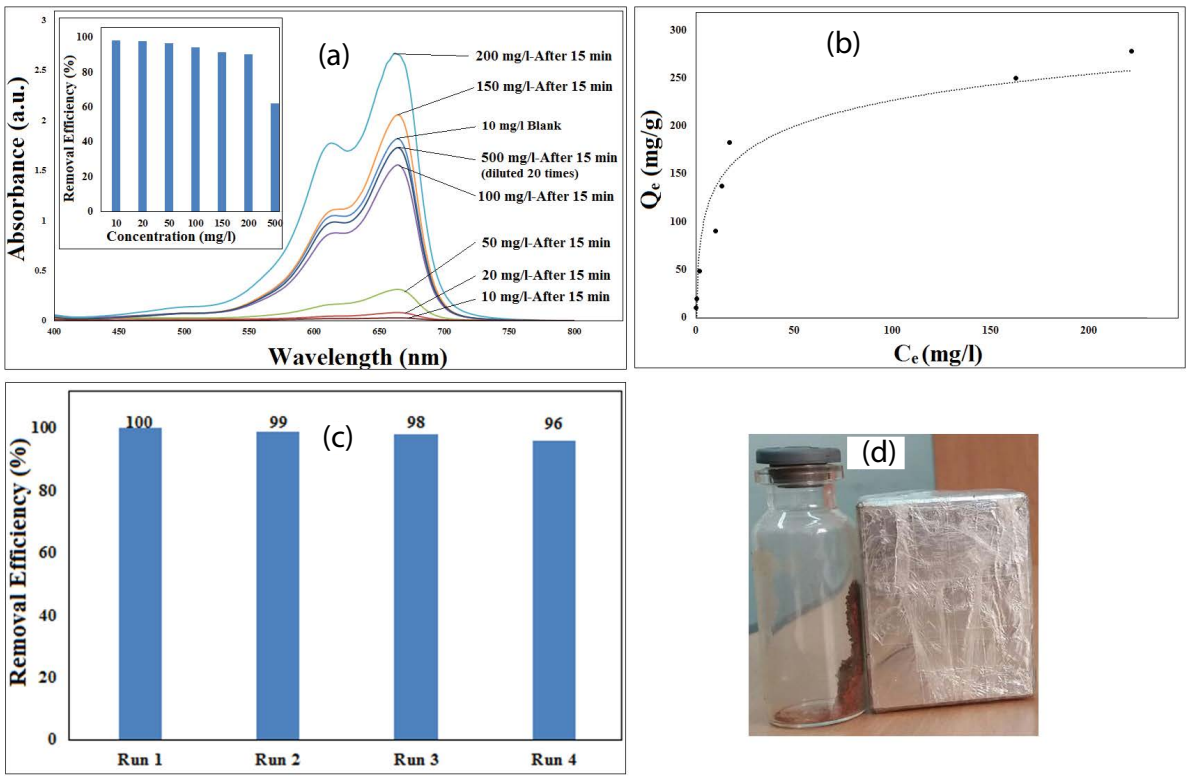

Fig. 3. (a) Adsorption activities for the decolorization of MB aqueous solution with mesoporous $ZnFe_2O_4$ (Inset: The removal efficiency of MB from aqueous solution with mesoporous $ZnFe_2O_4$), (b) Effect of dye concentrations on the equilibrium adsorption capacity of mesoporous $ZnFe_2O_4$, (c) Reusability of mesoporous $ZnFe_2O_4$, and (d) The magnetic responsiveness under an external magnetic field.

The effects of pH on removal efficiency of dyes were investigated with a vast pH range 3–11 (Fig. 4b). The results display that acidic pH does not support removal process. On the other hand, the best results were achieved in neutral and alkaline pHs. In that pHs, the efficiency reached was 100%. Therefore, these results suggest that alkaline and neutral initial pH values are beneficial for dye removal. Thus, pH 7 is selected as optimum pH for the other experiments.

3.3. Mechanism of adsorption

In order to investigate the mechanism of adsorption, kinetic models such as pseudo-first-order and pseudo-second-order can be used. The pseudo-first-order kinetic model (Eq. (11)) and pseudo-second-order model (Eq. (12)) are represented by the following equations:

$$\log\left(q_e - q_t\right) = \log q_e - \left(\frac{k_1}{2.303}\right)t \tag{11}$$

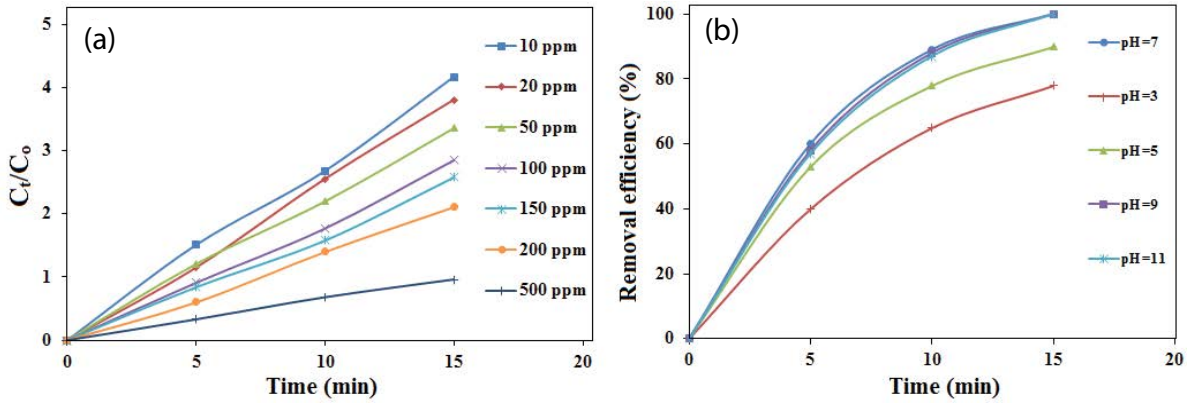

Fig. 4. (a) Remove of MB in the different concentrations and (b) the effect of pH on MB removal yield.

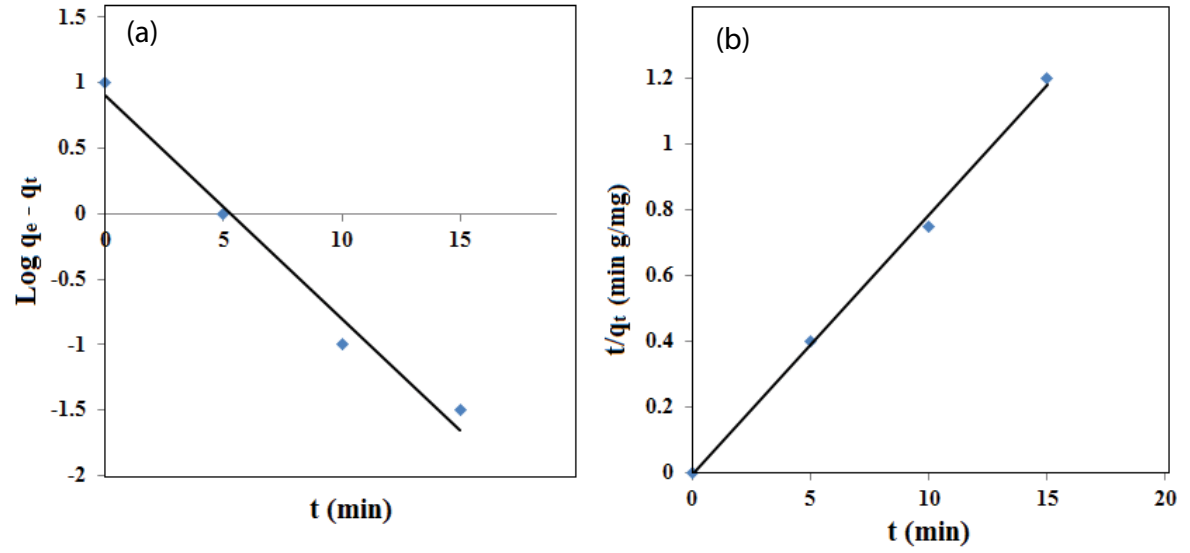

Fig. 5. Adsorption kinetics of MB over the $ZnFe_2O_4$ (a) pseudo-first-order and (b) pseudo-second-order kinetics.

Table 1
Kinetic parameters for adsorption of MB onto $ZnFe_2O_4$

Pseudo-first-order				Pseudo-second-order			
$q_{e,(exp)}$	k_1	$q_{e,cal}$	R^2	k_2	$q_{e,cal}$	H	R^2
12.5	0.267	1.28	0.979	1.018	12.46	165.1	0.997

$$\frac{t}{q_e} = \frac{1}{k_2 q_e^2} + \frac{1}{q_e} t \tag{12}$$

Amounts of MB adsorbed onto adsorbent at equilibrium and any time t (min) are shown as q_e and q_t (mg/g), respectively. k_1 (h^{-1}) and k_2 ((g/mg)/min) are first-order rate constant and second-order rate constant, respectively. Plotting the experimental data in the form of log ($q_e - q_t$) vs. t or t/q_t against t (min), a straight line would be acquired if the kinetic model is a convenient statement.

Table 2
Comparison of $ZnFe_2O_4$ with different morphology for removal of different pollutants

Morphology of $ZnFe_2O_4$	Pollutant	Removal efficiency (%)	Time	Reference
Hollow fiber	Acid dye	100[a]	17 h	[16]
Spherical	Phenol	68[b]	40 min	[24]
Spherical	Congo Red	98[c]	24 h	[25]
Spherical	Methylene blue	28[d]	3 h	[26]

[a]Dye concentration: 60 mg/L, adsorbent amount: 0.25 g.
[b]Dye concentration: 20 mg/L, adsorbent amount: 0.03 g.
[c]Dye concentration: 34.8 mg/L, adsorbent amount: 0.12 g.
[d]Dye concentration: 10 mg/L, adsorbent amount: 0.05 g.

Figs. 5a and b illustrate linear regression and the parameters are listed in Table 1. The pseudo-second-order adsorption mechanism is predominant for this adsorbent system. In addition, the theoretical value $q_{e,cal}$ obtained by

pseudo-second-order (12.5 mg/g) agrees experimental value $q_{e,\exp}$ (12.46 mg/g) well. The results can be concluded that the rate of MB adsorption process is controlled by the chemical reaction.

Mesoporous $ZnFe_2O_4$ adsorbent has different morphologies. Moreover, this catalyst has been used for the removal of different kind of pollutants. In Table 2, some examples of efficiency of $ZnFe_2O_4$ in different conditions are provided.

4. Conclusion

Mesoporous $ZnFe_2O_4$ was synthesized via a simple route in the presence of CMC as a green and nontoxic surfactant. The adsorption capacity of mesoporous $ZnFe_2O_4$ of methylene blue in aqueous solution was studied, which showed the maximum adsorption capacity of 250 mg/g. Also the mesoporous $ZnFe_2O_4$ can be easily recovered by applying an external magnetic field. Because of their superparamagnetic behavior, the adsorbent was quickly separated from wastewater. Therefore this magnetic mesoporous ferrite could be a good choice to adsorb contaminants from aqueous solutions.

References

[1] R. Rahimi, H. Kerdari, M. Rabbani, M. Shafiee, Synthesis, characterization and adsorbing properties of hollow Zn-Fe_2O_4 nanospheres on removal of Congo red from aqueous solution, Desalination, 280 (2011) 412–418.

[2] Y. Wang, F. Liu, Q. Yang, Y. Gao, P. Sun, T. Zhang, G. Lu, Mesoporous $ZnFe_2O_4$ prepared through hard template and its acetone sensing properties, Mater. Lett., 183 (2016) 378–381.

[3] T. Mathe, T. Moyo, J. Msomi, Optical properties of $Zn_{0.5}$ (Ni, Co)$_{0.5}$ Fe_2O_4 mixed spinel ferrite thin films, Phys. Status Solidi C, 5 (2008) 591–593.

[4] A.A. Hossain, H. Tabata, T. Kawai, Magnetoresistive properties of $Zn_{1-x}Co_xFe_2O_4$ ferrites, J. Magn. Magn. Mater., 320 (2008) 1157–1162.

[5] J. Yan, S. Gao, C. Wang, B. Chai, J. Li, G. Song, S. Chen, A facile electrospinning and direct annealing method for the fabrication of multi-porous $ZnFe_2O_4$ nanotubes with enhanced photocatalytic activity, Mater. Lett., 184 (2016) 43–46.

[6] M. Zhao, S. Fan, J. Liang, Y. Liu, Y. Li, J. Chen, S. Chen, Synthesis of mesoporous grooved $ZnFe_2O_4$ nanobelts as peroxidase mimetics for improved enzymatic biosensor, Ceram. Int., 41 (2015) 10400–10405.

[7] L. Fan, Y. Zhou, W. Yang, G. Chen, F. Yang, Electrochemical degradation of aqueous solution of Amaranth azo dye on ACF under potentiostatic model, Dyes Pigm., 76 (2008) 440–446.

[8] M. Rabbani, M. Heidari-Golafzani, R. Rahimi, Synthesis of TCPP/$ZnFe_2O_4$@ZnO nanohollow sphere composite for degradation of methylene blue and 4-nitrophenol under visible light, Mater. Chem. Phys., 179 (2016) 35–41.

[9] E. Oguz, B. Keskinler, Comparison among O_3, PAC adsorption, O_3/HCO_3^-, O_3/H_2O_2 and O_3/PAC processes for the removal of Bomaplex Red CR-L dye from aqueous solution, Dyes Pigm., 74 (2007) 329–334.

[10] J.C. Lopez-Montilla, S. Pandey, D.O. Shah, O.D. Crisalle, Removal of non-ionic organic pollutants from water via liquid–liquid extraction, Water Res., 39 (2005) 1907–1913.

[11] S. Kumar, R.R. Nair, P.B. Pillai, S.N. Gupta, M. Iyengar, A. Sood, Graphene oxide–$MnFe_2O_4$ magnetic nanohybrids for efficient removal of lead and arsenic from water, ACS Appl. Mater. Interfaces, 6 (2014) 17426–17436.

[12] C. Wu, J. Tu, C. Tian, J. Geng, Z. Lin, Z. Dang, Defective magnesium ferrite nano-platelets for the adsorption of As(V): the role of surface hydroxyl groups, Environ. Pollut., 235 (2018) 11–19.

[13] Z. Jia, Q. Qin, J. Liu, H. Shi, X. Zhang, R. Hu, S. Li, R. Zhu, The synthesis of hierarchical $ZnFe_2O_4$ architecture and their application for Cr(VI) adsorption removal from aqueous solution, Superlattices Microstruct., 82 (2015) 174–187.

[14] C.L. Warner, W. Chouyyok, K.E. Mackie, D. Neiner, L.V. Saraf, T.C. Droubay, M.G. Warner, R.S. Addleman, Manganese doping of magnetic iron oxide nanoparticles: tailoring surface reactivity for a regenerable heavy metal sorbent, Langmuir, 28 (2012) 3931–3937.

[15] Y.J. Tu, T.S. Chan, H.W. Tu, S.L. Wang, C.F. You, C.K. Chang, Rapid and efficient removal/recovery of molybdenum onto $ZnFe_2O_4$ nanoparticles, Chemosphere, 148 (2016) 452–458.

[16] J. Li, D.H. Ng, P. Song, Y. Song, C. Kong, Bio-inspired synthesis and characterization of mesoporous $ZnFe_2O_4$ hollow fibers with enhancement of adsorption capacity for acid dye, J. Ind. Eng. Chem., 23 (2015) 290–298.

[17] M. Sun, Y. Chen, G. Tian, A. Wu, H. Yan, H. Fu, Stable mesoporous $ZnFe_2O_4$ as an efficient electrocatalyst for hydrogen evolution reaction, Electrochim. Acta, 190 (2016) 186–192.

[18] D. Gherca, R.G. Ciocarlan, D.G. Cozma, N. Cornei, V. Nica, I. Sandu, A. Pui, Influence of surfactant concentration (carboxymethylcellulose) on morphology and particle sizes of cobalt nanoferrites, Struc., Rev. Chim., 14 (2013) 15.

[19] L. Hou, H. Hua, L. Lian, H. Cao, S. Zhu, C. Yuan, Green template-free synthesis of hierarchical shuttle-shaped mesoporous $ZnFe_2O_4$ microrods with enhanced lithium storage for advanced Li-ion batteries, Chem. Eur. J., 21 (2015) 13012–13019.

[20] X.B. Zhong, Z.Z. Yang, H.Y. Wang, L. Lu, B. Jin, M. Zha, Q.C. Jiang, A novel approach to facilely synthesize mesoporous $ZnFe_2O_4$ nanorods for lithium ion batteries, J. Power Sources, 306 (2016) 718–723.

[21] M. Su, C. He, V.K. Sharma, M.A. Asi, D. Xia, X.-z. Li, H. Deng, Y. Xiong, Mesoporous zinc ferrite: synthesis, characterization, and photocatalytic activity with H_2O_2/visible light, J. Hazard. Mater., 211 (2012) 95–103.

[22] R. Rameshbabu, R. Ramesh, S. Kanagesan, A. Karthigeyan, S. Ponnusamy, Synthesis of superparamagnetic $ZnFe_2O_4$ nanoparticle by surfactant assisted hydrothermal method, J. Mater. Sci.: Mater. Electron., 24 (2013) 4279–4283.

[23] S.-H. Yu, T. Fujino, M. Yoshimura, Hydrothermal synthesis of $ZnFe_2O_4$ ultrafine particles with high magnetization, J. Magn. Magn. Mater., 256 (2003) 420–424.

[24] W. Shi, F. Guo, H. Wang, C. Liu, Y. Fu, S. Yuan, H. Huang, Y. Liu, Z. Kang, Carbon dots decorated magnetic $ZnFe_2O_4$ nanoparticles with enhanced adsorption capacity for the removal of dye from aqueous solution, Appl. Surf. Sci., 433 (2018) 790–797.

[25] C. Muntean, M. Stoia, P. Barvinschi, Synthesis of nanocrystalline $ZnFe_2O_4$ and its use for the removal of Congo Red from aqueous solutions, Environ. Eng. Manage. J., 12 (2013) 959–967.

[26] R. Rahimi, M. Heidari-Golafzani, M. Rabbani, Preparation and photocatalytic application of $ZnFe_2O_4$@ZnO core–shell nanostructures, Superlattices Microstruct., 85 (2015) 497–503.